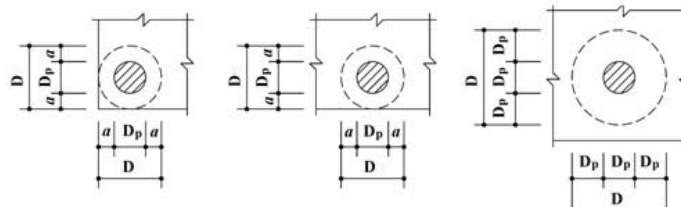


cross-section, the specially improved Lu’s method proposed by Lu (2001) is applied. And ratio refers to the utilization rate of strut, qarch represents the force of strut, Larch is the length of strut, DiaArchmin is the minimum diameter between upper and under cross-section, and  $f_t$  is concrete design tension strength.

$$\text{ratio} = \frac{100 \times \text{qarch}}{(\pi \times \text{DiaArchmin} \times \text{Larch} \times (1 + 0.4 \times (D/\text{DiaArchmin} - 1)) \times f_t)} \quad (3)$$

Meanwhile, D is effective restraint diameter, and should be valued as follows.

- 1 If the area of upper cross-section is bigger than that of under cross-section  
The value of D is shown in Fig.4.



**Fig. 4. Definition of D.**

- 2 If the area of upper cross-section is smaller than that of under cross-section

$$D = 3 \times \text{DiaArchmin} \quad (6)$$

**Ties setting**

The various arrangement of reinforcement have a great influence on the setting of ties and nodes upon piles. As concrete tensile strength is hard to be valued, reinforcements in a certain scope instead plays the key of ties, resulting in a condition that the scope of bars is beyond the size of exact ties.

*Scope of ties*

As the tensile strength of concrete lacks quantitative calculation and it is too small to be taken into consideration, the scope of ties and the form of reinforcement are the key to tensile strength of ties. According to Guo (2004) and their series of experiments, the best scope turns out to be twice the diameter of the pile (or equivalent diameter if it is a square pile).

*Node setting*

However, the width of a tie corresponds with the width of the node upon pile. Meanwhile, the height of the node upon pile is settled by  $a_s$ , the height of reinforcements. As the piles are square piles with a side length  $W_p$ , the length and width of a node upon piles is  $W_p$ , and the height is  $2a_s$ .

**Pile force reaction**

Most traditional models suppose that caps are absolute rigid, which resulted in an inaccurate inner force distribution. Lu (2012) supposes that the distribution of pile

reaction force relies on the stiffness, or the thickness. In addition, the checking programs are developed from experiments containing of the surveillance of field pile reaction force. Thus, solution to the distribution is as follows.  $k$  is the ratio of side pile's reaction force to total piles' reaction force.

1 When there is field measurement data of pile reaction force,  $k$  follows the surveillance.

2 When  $h \geq s \left( \frac{26.6Kp}{Ec \times b} \right)^{\frac{1}{3}}$ , the cap is rigid and  $k=1/6$ .

$h < s \left( \frac{26.6Kp}{Ec \times b} \right)^{\frac{1}{3}}$ , the cap is elastic and  $k=1/4$ .

$S$  is the distance between side pile and corner pile,  $b$  is the width of the cap,  $Kp$  is Pile vertical support stiffness, and  $E_c$  is the elastic modulus of concrete.

### Process of optimization

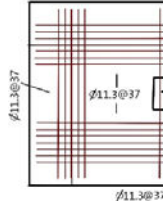
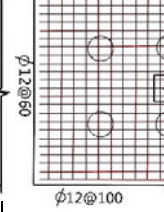
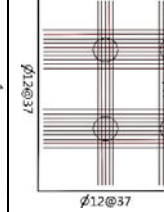
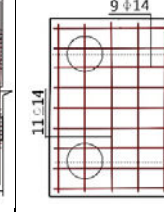
To reach the best match where all the utilization rates of nodes (nodes under column and nodes upon pile), strut and tie stay at a very high level, two iterative loops are applied in Matlab environment. The outer loop controls the gradual increase of load  $q$  while inner iterative loop optimizes the model at a specific load  $q$ . The controls of the inner iterative loop are  $Wc1$ ,  $Wc2$ ,  $Wcmid1$ ,  $Wcmid2$ ,  $a_s$ , and  $a_c$ .

### Comparison

The comparison with indoor model samples could evaluate the validity and accuracy of the method. Four samples (S6-1 from Adebar 1990, S6-2, S6-3 from Guo 2004 and S6-4 from Lu 2012) are simulated respectively in the checking program.

*Samples*

**Table 2. Parameters of Each Sample**

	<b>S6-1</b>	<b>S6-2</b>	<b>S6-3</b>	<b>S6-4</b>
Length (mm)	2600	2160	2160	1440
Width (mm)	1700	1435	1435	900
Height (thickness of protective layer)	600(100)	360(100)	360(100)	320(30)
Diameter of pile (mm)	200	180	180	180
Size of column (mm)	300×300	220×220	220×220	540×120
Corner pile reaction force (kN)	150	132.2	219.8	q/8
Side pile reaction force (kN)	1150	360	310.5	q/4
Ultimate compressive strength (MPa)	27.1	19.7	20.4	18.8
Splitting tensile strength (MPa)	3.71	1.53	1.56	1.63
Ultimate strength of bar (MPa)	610	460	460	591
Bar diameter (mm)	A11.3	A12	A12	A 14
Reinforcement form				

### Results

Cal means the results calculated, Exp represents the parameters of samples. And  $x(y)$  refers to the amount of reinforcement in  $x(y)$  direction within the scope of a tie. Meanwhile,  $y$  in middle means the amount of reinforcement across side piles in  $y$  direction. Ultra means overly reinforced.

**Table 3. Outputs and Comparison**

		Destruction condition (ratio %)					Reinforcement			
		Strut	Upper Node	Down Node	Tie	Breaking Load	X	Y	y in middle	Stirrups
S6-1	Cal	99.91	47.56	86.42	100	2750	3A11.3	2A11.3	13A11.3	2A11.3
	Exp	100	--	--	Ultra	2892	21A11.3	13A11.3	12A11.3	None
S6-2	Cal	100.3	88.58	93.40	100	1220	3A12	2A12	4A12	3A12
	Exp	100	--	--	Ultra	1250	7A12	4A12	4A12	None
S6-3	Cal	98.92	86.20	97.07	100	1380	4A12	2A12	5A12	4A12
	Exp	100	--	--	Ultra	1500	10A12	5A12	8A12	None
S6-4	Cal	101.9	47.85	98.85	100	1200	2A14	1A14	3A14	2A12
	Exp	100	--	--	Ultra	1462	3A14	3A14	3A14	None

### Conclusion

- 1 The numerical method approves a high accuracy, as all the ratios calculated have reached 90% or higher and all the failure modes estimated are splitting failure which correspond with those under model test condition. Moreover, the much more economic arrangement of reinforcement and higher utilization of each member prove that traditional arrangement of reinforcement needs urgent improvements.
- 2 Unlike traditional ambiguous models, the simulation is precise and applicable for various six-pile caps with diverse load type (better optimized nodes under column), different thickness (adaptive model type), various stiffness (precisely distributed pile reaction force) and irregular inclined strut (various cross-section strut).
- 3 The node offers a rational explanation for the different failure load of the same cap with various reinforcement arrangements. The variable length  $D$  and  $\theta$  make the model change with reinforcement form, while such is immutable in traditional model. Moreover, according to the comparison, solutions and parameters filtered from previous researches are composited together and work

accurately. On the contrary, all the parameters and solutions can be control variables respectively in turn, and thus, a much more rational parameter can be researched in the future.

- 4 As it turns out that only few stirrup is needed, the concrete tensile strength plays a role of stirrup between struts. However, the calculation scope of concrete tensile strength is ambiguous and the corresponding calculation is inaccurate. In that case, a much more accurate solution for concrete tensile strength needs a deeper exploring. Moreover, caps with pile group under more complex load is not discussed. And web reinforcement is ignored in the model, which has a non-ignorable effect on the bearing capacity of struts.

### ACKNOWLEDGMENTS

The research was supported by the National Key Basic Research Program of China (2013CB036304) and the National Key Technology R&D Program (2011BAG07B01).

### REFERENCE

- ACI 318-08, American Concrete Institute, January 2008.
- Adebar, P., Kuchma, D., and Collins M.P. (1990) “Strut-and-Tie Models for the Design of Pile Caps: An Experimental Study”, *ACI Structural Journal*, V. 87, No.1, January-February, pp. 81-92.
- Guo-liang Dai, Jian-feng Lu and Wei-ming Gong, (2012). *Theory and experiments of strut and tie model in thick cap*. China building industry press.
- EN 1992-1-1:2004, Eurocode 2: Design of Concrete Structures – Part 1-1: General rules and rules for buildings, December 2004.
- GAUTIER CHANTELOT and ALEXANDER MATHERN. (2010). “Strut-and-tie modelling of reinforced concrete pile caps”. Sweden, Department of Civil and Environmental Engineering, CHALMERS UNIVERSITY OF TECHNOLOGY.
- Hong-lei Guo, Da-jun Ding, and Yuan-han Wang. (2004). “Mechanism study of force in thick cap”. *Journal of Zhengzhou University (Engineering Science)*. Vol.25. No.1.
- Jian-feng Lu, Yong-sheng Jiang, and Shu-ting Liang. (2012). “Research in mechanical performance of six pile cap under concrete wall”. *Industrial Construction*. 42(2): 74-77, 32.
- Jian-feng Lu. (2001). “Research on design of pile cap using spatial truss action”. Department of Civil Engineering, Southeast University.
- Zong-zhong Ma, Ke-rong Zhou. (2006). “Study of Transfer Mechanism and Design Method of Thick Pile Caps”. *Structural Engineers*. Vol.22, No.3.

## Reverse Time Migration based Ultrasonic Wave Detection for Concrete Structure

Mingshun Hu<sup>1</sup>, Shen-en Chen<sup>2</sup>, and Dongming Pan<sup>3</sup>

<sup>1</sup> Ph.D Student, School of Resource and Geosciences, China University of Mining and Technology, Xuzhou, Jiang Su, China, 221116; [mingshunhu1985@gmail.com](mailto:mingshunhu1985@gmail.com)

<sup>2</sup> Professor, Department of Civil and Environmental Engineering, University of North Carolina at Charlotte, Charlotte, NC, USA, 28223; [schen12@uncc.edu](mailto:schen12@uncc.edu)

<sup>3</sup> Professor, School of Resource and Geosciences, China University of Mining and Technology, Xuzhou, Jiang Su, China, 221116; [pdm3816@163.com](mailto:pdm3816@163.com)

**ABSTRACT:** Ultrasonic wave testing is a classic NDT method to detect, locate and monitor the crack/fracture in construction materials. In this paper, a new ultrasound data interpretation technique is introduced: The reverse time migration (RTM) is a wave equation based pre-stack method used in seismic exploration. Since RTM can utilize all kinds of waves, such as reflection waves, refraction waves and diffraction waves, it has no dip limits in migration and can image the inside of complicated structures. However, the large data generation and sophisticated velocity field analysis are the bottlenecks for RTM that hinder its wide applications. A hybrid boundary condition (including random boundary and absorption boundary simultaneously) is suggested in this paper to reconstruct the source wave field to address the memory storage issues. A numerical model with S-shaped internal fracture is presented to demonstrate the technique for detection of internal flaws. The results indicate that the accuracy of detecting the embedded flaw within construction material is affected by the sampling space and the range of wave frequency.

### INTRODUCTION

Defects and damage affect the performance of structures and nondestructive testing (NDT) techniques such as ultrasonic testing has been applied to detect defects: Bogas et al (2013) evaluated the compressive strength of structural lightweight aggregate concrete mixes by ultrasonic pulse velocity (UPV) method; Dilek (2007) applied UPV in field detection of damage to concrete in service and field quality assessment of cast-in-place concrete and masonry under construction; Mohammed et al (2011) applied both UPV and rebound hammer tests to evaluate the rubbercrete; and finally, Acciani et al (2010) used finite element simulation to study ultrasonic wave propagation in concrete structures with defects.

Most ultrasound data processing used straight-forward peak amplitude or initial arrival methods. More advanced techniques such as the frequency compounding method (Ho *et al.* 2012) and artificial neural network and adaptive neuro-fuzzy inference system have been used (Bilgehan 2011). Bui and Kodjo (2013) suggested that ultrasonic travel time shift is more sensitive when used in an indirect configuration of transmission than in a semi-direct configuration in evaluation of concrete distributed cracks.

Reverse time migration is a wave equation based pre-stack migration method used in geophysical exploration (Baysal *et al.* 1983, Levin 1984, Chang and McMechan 1987, Guan *et al.* 2009). RTM method has been suggested for structure defect detection (Lin and Yuan 2001, Lin and Yuan 2005) (Anderson *et al.* 2011, Saenger *et al.* 2011). However, classical RTM method has two fundamental issues: 1) large computer memory is required for saving forward source wavefield, and 2) difficulty in velocity analysis.

To improve on the classical RTM, this paper tries to simulate the acoustic wave propagation in concrete with various defects by a time second order and space tenth order rectangle grid finite

difference approximation to study the wavefield characteristics when acoustic wave hit these defects. We then used hybrid boundary condition combined with perfectly matched layer (PML) absorbing boundary condition and random boundary condition to address the memory issue. To demonstrate the effect of the modified method, two numerical concrete models with complicated defects are presented.

## PROPAGATION OF ACOUSTIC WAVE

### Acoustic wave equation

We start by stating the two-dimensional acoustic wave equation as (Feyman 1970):

$$\frac{\partial^2 P}{\partial x^2} + \frac{\partial^2 P}{\partial y^2} - \frac{1}{v^2} \frac{\partial^2 P}{\partial t^2} = 0 \quad (1)$$

where  $P$  is the acoustic pressure,  $t$  is time and  $v$  is the speed of acoustic wave. When external source  $s(t)$  is put at the position  $(x_0, y_0)$  within the two dimensional space  $(x, y)$ , equation (1) can be rewritten as

$$\frac{\partial^2 p}{\partial x^2} + \frac{\partial^2 p}{\partial z^2} - \frac{1}{v^2} \frac{\partial^2 p}{\partial t^2} + s(t, x_0, y_0) = 0 \quad (2)$$

Above acoustic wave equations are derived on the assumption of homogenous media. For concrete material, the acoustic velocities typically range from 2000m/s to 5500m/s (Krautkramer and Krautkramer 1990). In ultrasonic testing of concrete and cement, the range of the frequency is from 50 to 500 kHz.

### Finite-difference solution

In rectangular coordinate, the second order difference approximation of  $p=p(x, z, t)$  respect to time  $t$  is

$$\frac{\partial^2 p_{ij}^n}{\partial t^2} = \frac{1}{\Delta t^2} [p_{ij}^{n+1} + p_{ij}^{n-1} - 2p_{ij}^n] \quad (3)$$

where  $i, j$  and  $n$  are the discrete sequence number with respect to  $x, z$  and  $t$ .  $\Delta x$  and  $\Delta z$  are the grid space in the  $x$  and  $z$  direction.  $\Delta t$  is time step. Here we can obtain the  $2N$  order difference schemes of  $\frac{\partial^2 p}{\partial x^2}$  and  $\frac{\partial^2 p}{\partial z^2}$  as,

$$\begin{aligned} \frac{\partial^2 p_{ij}^n}{\partial x^2} &= \frac{1}{\Delta x^2} \left[ \sum_{l=1}^N a_l (p_{i+l,j}^n + p_{i-l,j}^n) + a_0 p_{ij}^n \right] \\ \frac{\partial^2 p_{ij}^n}{\partial z^2} &= \frac{1}{\Delta z^2} \left[ \sum_{l=1}^N a_l (p_{i,j+l}^n + p_{i,j-l}^n) + a_0 p_{ij}^n \right] \end{aligned} \quad (4)$$

where  $a_l$  represent difference coefficients. When  $N$  is 5, we have  $a_0 = -\frac{5269}{1800}$ ,  $a_1 = \frac{5}{3}$ ,  $a_2 = -\frac{5}{21}$ ,

$a_3 = \frac{5}{126}$ ,  $a_4 = -\frac{5}{1008}$  and  $a_5 = \frac{5}{3150}$ . Hence, equation (3) can be rewritten in difference scheme as,

$$p_{ij}^{n+1} = 2p_{ij}^n - p_{ij}^{n-1} + \frac{v^2 \Delta t^2}{\Delta x^2} \left[ \sum_{l=1}^N a_l (p_{i+l,j}^n + p_{i-l,j}^n) + a_0 p_{ij}^n \right] + \frac{v^2 \Delta t^2}{\Delta z^2} \left[ \sum_{l=1}^N a_l (p_{i,j+l}^n + p_{i,j-l}^n) + a_0 p_{ij}^n \right] + v^2 \Delta t^2 s(n\Delta t) \quad (5)$$

where  $S(n\Delta t)$  is discrete source function. Equation (5) represents the acoustic wave in forward propagation. Similarly, the difference formula of acoustic wave in backward propagation is

$$p_{ij}^{n-1} = 2p_{ij}^n - p_{ij}^{n+1} + \frac{v^2 \Delta t^2}{\Delta x^2} \left[ \sum_{l=1}^N a_l (p_{i+1,j}^n + p_{i-1,j}^n) + a_0 p_{ij}^n \right] + \frac{v^2 \Delta t^2}{\Delta z^2} \left[ \sum_{l=1}^N a_l (p_{i,j+1}^n + p_{i,j-1}^n) + a_0 p_{ij}^n \right] \quad (6)$$

### Boundary condition

Using paraxial approximation, the boundary conditions are derived for the simulation that minimizes artificial reflections from the edges of the domain of computation. In this way acoustic and elastic wave propagation in a limited area can be efficiently used to describe physical behavior in an unbounded domain (Clayton and Engquist 1977). Another nonreflecting boundary condition for discrete acoustic and elastic wave equation was applied (Cerjan et al. 1985).

Berenger (1994) first proposed the absorbing boundary condition using perfectly matched layer (PML), which has become a popular method in acoustic wave numerical simulation. The governing equation of PML is

$$\begin{aligned} p &= p_x + p_z \\ \frac{\partial p_x}{\partial t} + d_x(x)p_x &= v^2 \frac{\partial A_x}{\partial x} \\ \frac{\partial p_z}{\partial t} + d_z(z)p_z &= v^2 \frac{\partial A_z}{\partial z} \\ \frac{\partial A_x}{\partial t} + d_x(x)A_x &= \frac{\partial p_x}{\partial x} + \frac{\partial p_z}{\partial x} \\ \frac{\partial A_z}{\partial t} + d_z(z)A_z &= \frac{\partial p_x}{\partial z} + \frac{\partial p_z}{\partial z} \end{aligned} \quad (7)$$

where pressure  $p$  is divided into two terms,  $p_x$  and  $p_z$  for pressure in x-direction and z-direction, respectively.  $d_x(x)$  and  $d_z(z)$  are the attenuation factors. The effectiveness of PML boundary absorbing is relative to the attenuation factors. Based on Berenger, Hastings derived the attenuation factor in x-direction as (Hastings *et al.* 1996),

$$d_x(l) = \frac{(n+1)v}{2\delta} \ln\left(\frac{1}{R}\right) \left(\frac{l}{\delta}\right)^n \quad (8)$$

where  $\delta$  is the thickness of the PML absorbing boundary,  $l$  is the distance between the wave head and inner boundary in x-direction.  $R$  is an ideal reflection coefficient of boundary (generally,  $R = 10^{-3} \sim 10^{-6}$ ).  $v$  is the velocity of compressional wave,  $n$  is the order of the attenuation function (generally,  $n = 1, 2, \dots, 4$ ). This paper assumes  $R = 10^{-6}$  and  $n = 1$ .

Since huge memory space is needed for saving the forward source field in RTM, Clapp(2009) replaced absorbing boundary by random boundary, which effectively save the wavefield information into last snapshot. However, random boundary condition highly increased the computation cost and, if we set all four sides as random boundary when source and receivers are also placed near boundary, severe random noise would be created. To solve this issue, a compromised hybrid boundary condition, combined with PML and random boundary condition, will be applied in this paper.

### PRINCIPLE OF REVERSE TIME MIGRATION (RTM)

For forwardly propagating a source function within the computational domain from time  $t=0$  to  $t=\text{maxtime}$ , RTM stores the wavefield  $S(x,z,t)$  at time steps with time sampling at  $\Delta t$ . The

wave records is then injected into a second computational domain and propagated from  $t=\text{maxtime}$  to  $t=0$  and stored in  $R(x, z, t)$ . The final zero offset migrated image,  $I$ , is then constructed at each  $(x, z)$  location by cross-correlation (Claerbout 1971, Kaelin and Guitton 2006)

$$I(x, z) = \sum_{\text{time}} S(x, z, t) R(x, z, t) \quad (9a)$$

In normalized form with respect to the energy of source wavefield:

$$I(x, z) = \frac{\sum_{\text{time}} S(x, z, t) R(x, z, t)}{\sum_{\text{time}} S^2(x, z, t)} \quad (9b)$$

Using the modified scheme, it is not necessary to store wavefield  $S(x, z, t)$  at each time steps during forward computation. Only the wavefield value of the absorbing boundary area at each time step from  $t=0$  to  $t=\text{maxtime}$ , and last two snapshot, will be stored (Figure 1).

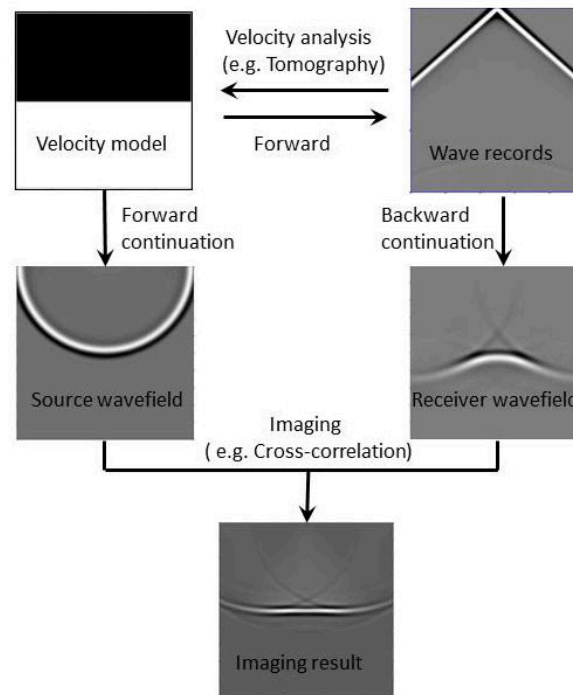


**FIG.1. Principle of reverse time migration**

## NUMERICAL SIMULATION EXAMPLE

A concrete beam with 300mm×400mm in  $x$ - $z$  section and acoustic wave velocity 4000m/s is assumed to have enclosed a complicated horizontal ‘S’ flaw with acoustic wave velocity 2000m/s. Sensor array (19 sensors with 25 mm spacing) is located at the top of the beam in a straight line. 5 sources locating on the position as shown in Figure 2.

### Wavefield continuation and reconstruction

Ten order rectangle two-dimensional ( $x$ - $z$ ) finite difference approximation is used to compute the ultrasonic wave propagation. The domain is discretized into grids of size 2mm×2mm. Ricker wavelet in time-domain is used as the source function,

$$s(t) = (1 - 2\pi^2 f_m^2 t^2) e^{-\pi^2 f_m^2 t^2} \quad (10)$$

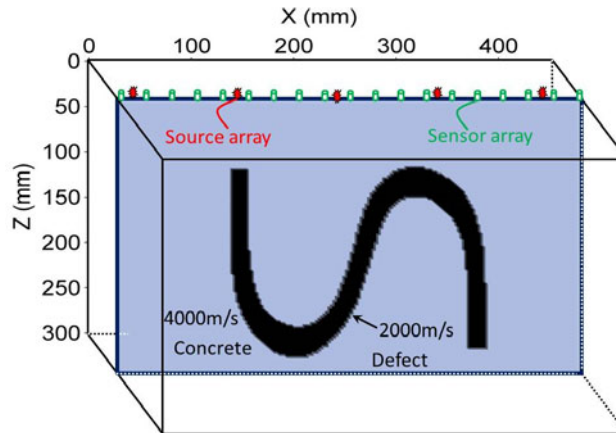


**FIG.2. Numerical model of concrete structure with 'S' defect**

where  $f_m$  is main frequency and is set at 150kHz with recorded time length of 300ms. For the stability of the two-dimensional acoustic wave 2N order finite difference scheme, it should meet the following stability condition (Liu *et al.* 1998):

$$v_{\max}(x, z) \cdot \Delta t \cdot \left( \frac{1}{\Delta x^2} + \frac{1}{\Delta z^2} \right)^{\frac{1}{2}} < \left( \sum_l^{N_1} a_{2l-1} \right)^{-\frac{1}{2}} \quad (11)$$

where  $v_{\max}(x, z)$  is max compressional velocity and  $N_1$  is the largest odd number but not greater than  $N$ .  $a$  represents coefficient of difference.

Figure 3 shows several forward snapshots corresponding to an initial wave front (first shot). We can see that there exist several diffractions when the waves propagate to the flaw. Hence it is tough to image the defective structure by conventional signal processing techniques. Therefore we cannot interpret the flaws by only reflection waves.

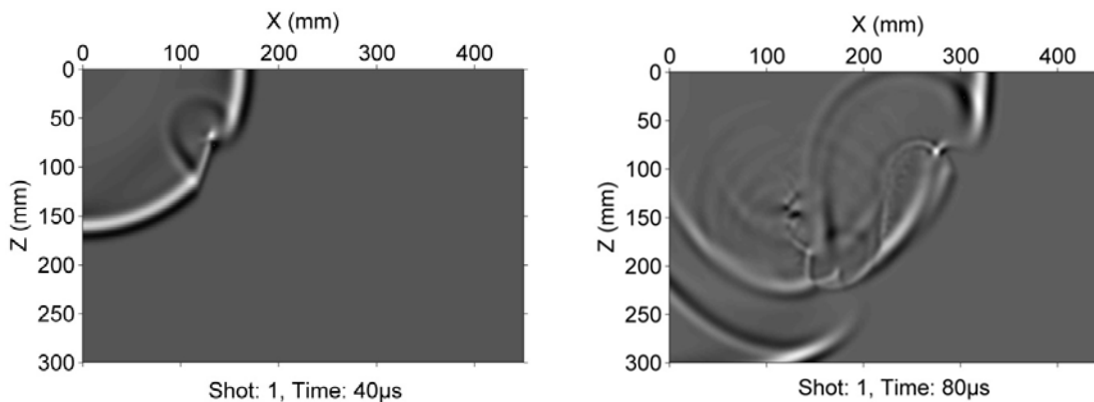


**FIG.3. Snapshots corresponding to first shot**

To improve the computation, we set the top boundary as PML absorbing condition (shown in Figure 4). To save the wavefront information, the other three boundaries are set as random conditions. In order to ensure wavefront reconstructed accurately, the wavefield value of top absorbing boundary should be saved as well as the last two snapshots of the source wavefront. It is not necessary, however, to save all top boundary wavefield values. It is only necessary to store the wavefield values of the layers. And the number of layers required can be determined by half